

Euphonium: Steering Video Flow Matching via Process Reward Gradient Guided Stochastic Dynamics

Ruizhe Zhong ^{*†1} Jiesong Lian ^{*†2} Xiaoyue Mi ³ Zixiang Zhou ⁴ Yuan Zhou ^{‡4} Qinglin Lu ⁴ Junchi Yan ^{§1}

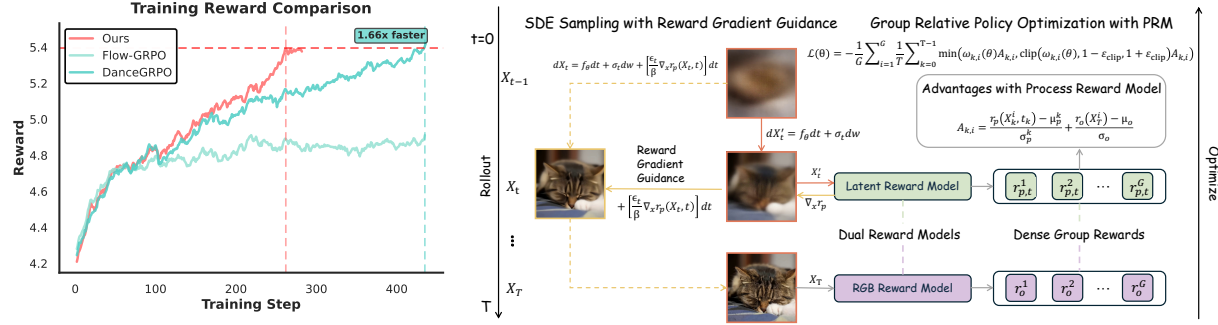


Figure 1. **Left:** Convergence Comparison. Euphonium converges **1.66×** faster than other baselines, reaching equivalent performance with fewer training steps. **Right:** Overview of the Euphonium pipeline.

Abstract

While online Reinforcement Learning has emerged as a crucial technique for aligning flow matching models with human preferences, current approaches are hindered by inefficient exploration during training rollouts. Relying on undirected stochasticity and sparse outcome rewards, these methods struggle to discover high-reward samples, resulting in data-inefficient and slow optimization. To address these limitations, we propose Euphonium, a novel framework that steers generation via process reward gradient guided dynamics. Our key insight is to formulate the sampling process as a theoretically principled Stochastic Differential Equation that explicitly incorporates the gradient of a Process Reward Model into the flow drift. This design enables dense, step-by-step steering toward high-reward regions, advancing beyond the unguided exploration in prior works, and theoretically encompasses existing sampling methods (e.g., Flow-GRPO, Dance-

GRPO) as special cases. We further derive a distillation objective that internalizes the guidance signal into the flow network, eliminating inference-time dependency on the reward model. We instantiate this framework with a Dual-Reward Group Relative Policy Optimization algorithm, combining latent process rewards for efficient credit assignment with pixel-level outcome rewards for final visual fidelity. Experiments on text-to-video generation show that Euphonium achieves better alignment compared to existing methods while accelerating training convergence by $1.66\times$.

1. Introduction

Flow matching (Lipman et al., 2022; Liu et al., 2022; Tong et al., 2023) has emerged as the dominant paradigm for high-fidelity video generation, underpinning leading systems such as Sora (OpenAI, 2025), Veo (DeepMind, 2025), Wan (Wan et al., 2025), Kling (Technology, 2025), and Seedance (Gao et al., 2025). While large-scale pre-training endows foundation models with remarkable generative capabilities, it is often insufficient for ensuring alignment with nuanced human preferences, such as specific aesthetic styles and prompt adherence. Consequently, post-training via Reinforcement Learning (RL) has become a critical frontier for bridging this alignment gap (Black et al., 2023).

^{*}Equal contribution [†]Work done during an internship at Tencent Hunyuan [‡]Project Leader [§]Shanghai Jiao Tong University ²Huazhong University of Science and Technology ³University of Chinese Academy of Sciences ⁴Tencent Hunyuan. Correspondence to: Ruizhe Zhong <zerzerzerz271828@sjtu.edu.cn>, Jiesong Lian <lian700@hust.edu.cn>, Junchi Yan <yan-junchi@sjtu.edu.cn>.

ative Policy Optimization, GRPO) to flow matching requires introducing stochasticity into the deterministic probability flow Ordinary Differential Equations (ODEs). Recent approaches like Flow-GRPO (Liu et al., 2025b) and DanceGRPO (Xue et al., 2025) address this by formulating Stochastic Differential Equations (SDEs) to enable policy exploration. Despite this progress, these methods rely on *undirected* stochastic dynamics: the model explores the latent space via random perturbations and receives feedback only after the entire video is generated. Consequently, discovering high-reward trajectories becomes exceedingly difficult, as random noise rarely steers generation toward the narrow manifold of high-quality samples. This inefficiency in exploration leads to sparse positive supervision, resulting in data-inefficient and slow optimization.

We posit that efficient alignment necessitates not merely stochastic exploration, but *guided* exploration. Rather than relying on undirected noise to fortuitously discover high-reward trajectories, the sampling process itself should be actively steered toward preferred regions. To this end, we propose **Euphonium** (Exploration Utilizing Process Heuristics Over Non-equilibrium Sampling), a principled framework grounded in the Non-Equilibrium Transport Sampling (NETS) formalism (Albergo et al., 2023; Albergo & Vanden-Eijnden, 2024). By defining a novel reward-augmented potential that integrates the flow prior with a dense Process Reward Model (PRM) (Lightman et al., 2023), we derive a theoretically grounded SDE where the reward gradient is explicitly incorporated into the flow drift. This design enables dense, step-by-step steering toward high-reward regions during exploration. Moreover, our formulation theoretically encompasses existing sampling methods (e.g., Flow-GRPO, DanceGRPO) as special cases when the reward term vanishes, providing a unified perspective on stochastic flow dynamics.

A potential concern with reward-guided exploration is the inference-time dependency on the reward model. We address this by deriving a distillation objective that internalizes the guidance signal into the flow network weights, enabling the deployed model to operate identically to the base generator without requiring an external reward model.

We instantiate this framework via a Dual-Reward GRPO algorithm, combining latent-space process rewards for efficient credit assignment with pixel-space outcome rewards for final visual fidelity alignment. Our main contributions are summarized as follows:

- **Guided Exploration via Process Reward Gradient.** We derive a reward-augmented stochastic dynamics that injects dense gradient signals from a Process Reward Model directly into the flow drift. This principled formulation enables active steering toward high-reward regions during exploration, and theoretically encom-

passes prior sampling strategies (e.g., Flow-GRPO, DanceGRPO) as reward-free special cases.

- **Dual-Reward Optimization.** We introduce a dual-reward training scheme that combines latent-space process rewards for efficient credit assignment with pixel-space outcome rewards for final visual fidelity alignment.
- **Reward-Gradient-Free Inference.** To eliminate inference-time dependency on the reward model after training, we derive a distillation objective that internalizes the guidance signal into the flow network weights, enabling deployment identical to the base generator.
- **Empirical Performance.** Euphonium achieves better alignment on VBench2 for text-to-video generation, outperforming existing post-training methods while accelerating training convergence by **1.66 \times** .

2. Related Works

2.1. Flow Matching

Flow matching (Lipman et al., 2022; Tong et al., 2023) has become one of the standards for video generation. Specifically, Rectified Flow (Liu et al., 2022; Esser et al., 2024) utilizes linear optimal transport (OT) paths to enforce straight trajectories, reducing inference steps.

2.2. Flow Model Alignment

To align generative models with human preferences, RL techniques developed for diffusion models (Black et al., 2023) have been adapted to flow matching. Existing methods generally fall into two paradigms: stochastic exploration and direct optimization.

Stochastic Exploration. A key challenge in applying RL to flow matching is the deterministic nature of the ODE sampler. Flow-GRPO (Liu et al., 2025b) addresses this by formulating a SDE to inject noise, enabling policy exploration around the probability flow. DanceGRPO (Xue et al., 2025) improves this with a shared-noise strategy to isolate policy-driven improvements, while MixGRPO (Li et al., 2025) adopts a mixed ODE-SDE strategy to reduce computational overhead. To mitigate the sparsity of outcome rewards, Chunk-GRPO (Luo et al., 2025) and E-GRPO (Zhang et al., 2026) propose step aggregation, while TempFlow-GRPO (He et al., 2025) and TreeGRPO (Ding & Ye, 2025) leverage branching structures for finer credit assignment. Despite these advances, these methods rely on undirected noise, exploring the latent space inefficiently without active guidance.

Direct Optimization. Distinct from stochastic RL, another paradigm utilizes reward gradients directly. ReFL (Xu et al.,

2023) performs direct backpropagation from the reward model through the denoising chain to update parameters. Furthermore, it requires ground truth samples for supervised regularization. VGG-Flow (Liu et al., 2025d) adopts an optimal control perspective, regressing the velocity field to match the gradient of a learned value function. However, these methods often rely on deterministic regression that limits diversity and exploration.

2.3. Guided Sampling and Process Supervision

Generative processes can also be steered via inference-time mechanisms. Early works like Classifier Guidance (Ho & Salimans, 2022) and energy-based guidance (Lu et al., 2023) modify the drift term based on conditioning. Process supervision, popularized in LLMs (Lightman et al., 2023), has been adapted to video generation. Video-T1 (Liu et al., 2025a) applies search-based methods using verifiers to prune low-quality branches. While VideoAlign (Liu et al., 2025c) pioneered the utilization of video generation models as latent reward models, its application was restricted to inference-time guidance. Building upon this latent supervision concept, PRFL (Mi et al., 2025) incorporates a process-aware latent reward model to optimize video generation during training via direct reward feedback learning. However, PRFL employs a deterministic sampling strategy and requires ground truth samples for supervised regularization.

3. Preliminaries

3.1. Flow Matching and Linear OT Paths

Let $p_{\text{data}}(x)$ denote the data distribution and $p_0(x) = \mathcal{N}(x; 0, I)$ be a standard Gaussian source distribution. Continuous Normalizing Flows (Lipman et al., 2022) define a probability path $p_t(x)$ for $t \in [0, 1]$ generated by a time-dependent vector field. We denote the optimal vector field as $u_t(x)$ and its neural network approximation as $u_\theta(x, t)$ with parameters θ . The flow $\phi_t(x)$ satisfies the ODE:

$$\frac{d}{dt} \phi_t(x) = u_t(\phi_t(x)), \quad \phi_0(x) = x. \quad (1)$$

Flow matching optimizes $u_\theta(x, t)$ to approximate the conditional vector field generating a target probability path. We adopt the Linear Optimal Transport (OT) conditional path:

$$X_t = (1 - t)X_0 + tX_1, \quad (2)$$

where $X_0 \sim p_0$ and $X_1 \sim p_{\text{data}}$. Under this path construction, the marginal score function $\nabla \log p_t(x)$ admits an explicit relationship with the velocity field $u_t(x)$.

Proposition 3.1 (Score-Velocity under Linear OT (Zheng et al., 2023)). *For the linear path $X_t = (1 - t)X_0 + tX_1$*

where $X_0 \sim \mathcal{N}(0, I)$, the score function of the marginal density $p_t(x)$ relates to the optimal velocity field $u_t(x)$ via:

$$\nabla \log p_t(x) = -\frac{x - tu_t(x)}{1 - t}. \quad (3)$$

Detailed proof is provided in Appendix A.

3.2. Non-Equilibrium Transport Sampling (NETS)

To enable step-wise guidance during the generation process, we formulate the sampling problem as sampling from a target density $q_t(x)$ defined by a Boltzmann-Gibbs distribution associated with a time-dependent potential $U_t(x)$ (Albergo & Vanden-Eijnden, 2024):

$$q_t(x) \propto \exp(-U_t(x)). \quad (4)$$

To sample from $q_t(x)$ while respecting the transport dynamics of the pre-trained flow, we utilize the Non-Equilibrium Transport Sampler (NETS) (Albergo & Vanden-Eijnden, 2024). The dynamics are governed by the following SDE:

$$dX_t = (u_\theta(X_t, t) - \epsilon_t \nabla U_t(X_t)) dt + \sqrt{2\epsilon_t} dW_t, \quad (5)$$

where $u_\theta(X_t, t)$ provides the base velocity, $-\nabla U_t$ acts as a conservative force guiding the particle towards low-potential regions, and ϵ_t is a time-dependent diffusion coefficient.

4. Methodology

In this section, we present our post-training algorithm for video generation grounded in online reinforcement learning. Our framework enhances the standard sampling process by introducing a PRM that guides exploration through the stochastic dynamics of Section 3. This guided exploration is integrated with dual-reward GRPO to align the flow matching model with human preferences. We first instantiate the framework by deriving guided dynamics for two potential structures (Section 4.1). We then detail Process Reward Model training (Section 4.2) and the complete online sampling and optimization pipeline (Section 4.3). Finally, we introduce a policy distillation formulation that explicitly internalizes reward guidance into the flow network, enabling efficient reward-gradient-free inference (Section 4.4).

4.1. Guided Dynamics for Specific Potentials

We now derive the update rules for distinct sampling scenarios by defining the specific structure of the potential $U_t(x)$ within the general SDE defined in Equation (5).

4.1.1. UNGUIDED STOCHASTIC SAMPLING

We first consider the case where the potential corresponds to the negative log-likelihood of the flow density:

$$U_t(x) = -\log p_t(x). \quad (6)$$

Substituting into Equation (5) yields the standard score-based diffusion term $\epsilon_t \nabla \log p_t(x)$. Invoking Proposition 3.1 and substituting the velocity u_θ gives:

$$dX_t = \left[\left(1 + \frac{t\epsilon_t}{1-t} \right) u_\theta(X_t, t) - \frac{\epsilon_t}{1-t} X_t \right] dt + \sqrt{2\epsilon_t} dW_t. \quad (7)$$

Remark. This formulation recovers the intrinsic stochastic dynamics of the flow model. Without external reward signals, our derivation naturally recovers the dynamics underlying methods such as DanceGRPO and Flow-GRPO. More details are provided in Appendix B.

4.1.2. REGULARIZED REWARD GUIDANCE

We adopt a more general setting: maximizing expected reward subject to a Kullback-Leibler (KL) divergence constraint against the reference policy π_{ref} . The objective is to find a policy π maximizing:

$$\mathcal{J}(\pi) = \mathbb{E}_{x \sim \pi}[r(x)] - \beta D_{\text{KL}}(\pi \| \pi_{\text{ref}}), \quad (8)$$

where β controls the KL penalty strength. The closed-form solution is the Boltzmann distribution (Appendix C):

$$\pi^*(x) = \frac{1}{Z} \pi_{\text{ref}}(x) \exp\left(\frac{r(x)}{\beta}\right), \quad (9)$$

where Z is the partition function.

To apply this result to our time-dependent generative process, we instantiate Equation (9) at each timestep t . Concretely, we identify the reference policy π_{ref} with the flow marginal $p_t(x)$ and the reward $r(x)$ with the PRM $r_p(x, t)$. The target density $q_t(x)$ then takes the form:

$$q_t(x) \propto p_t(x) \exp\left(\frac{r_p(x, t)}{\beta}\right). \quad (10)$$

According to Equation (4), we obtain:

$$U_t(x) = -\log p_t(x) - \frac{1}{\beta} r_p(x, t) + C_t, \quad (11)$$

where C_t is a constant independent of x .

Substituting into Equation (5) and applying Proposition 3.1, we obtain the KL-regularized dynamics:

$$\begin{aligned} dX_t = & \underbrace{\left[\left(1 + \frac{t\epsilon_t}{1-t} \right) u_\theta(X_t, t) - \frac{\epsilon_t}{1-t} X_t \right] dt}_{\text{Reference Dynamics}} \\ & + \underbrace{\left[\frac{\epsilon_t}{\beta} \nabla_x r_p(X_t, t) \right] dt + \sqrt{2\epsilon_t} dW_t.}_{\text{Reward Gradient Guidance}} \end{aligned} \quad (12)$$

Here, β governs the KL regularization strength. Higher β tightens adherence to the reference flow, while lower β permits stronger reward-gradient steering.

4.2. Training of the Process Reward Model

To provide dense, step-wise guidance via the potential $U_t(x)$, we train a PRM $r_\phi(x, t, c)$, where c denotes the text prompt. We adopt a latent-space design to circumvent the prohibitive memory costs of backpropagating through the video decoder and the high variance of zeroth-order gradient estimation (see Appendix D for detailed analysis). The PRM estimates the quality of intermediate latent states X_t throughout the generative trajectory.

Architecture. The PRM operates directly in the latent space, taking the noisy video latent x_t , timestep t , and text embeddings c as inputs. We initialize the PRM from a subset of the pre-trained DiT layers to leverage learned representations while reducing computational overhead. A lightweight MLP head projects the hidden states into a scalar reward score $s \in \mathbb{R}$. Both VAE and text encoder are frozen.

Noise Perturbation. During training, given a clean video latent $X_1 \sim p_{\text{data}}$, we sample a random timestep $t \sim \mathcal{U}[0, 1]$ and construct the perturbed latent X_t following the Linear OT path (Equation (2)). This perturbation strategy ensures that the reward surface r_ϕ is well-defined across the entire probability path, enabling reliable gradient estimation at arbitrary noise levels.

Training Objective. We adopt the Bradley-Terry model (Bradley & Terry, 1952) for preference learning. Given a pair of latents (X_1^w, X_1^l) where $X_1^w \succ X_1^l$, we sample a shared timestep t and noise ϵ to construct the perturbed pair (X_t^w, X_t^l) . The model is trained to assign higher reward to the preferred sample via pairwise ranking loss:

$$\mathcal{L}_{\text{BT}}(\phi) = -\mathbb{E}_{(X_1^w, X_1^l), t, \epsilon} [\log \sigma(r_\phi(X_t^w, t, c) - r_\phi(X_t^l, t, c))]. \quad (13)$$

4.3. Online Sampling and Training Pipeline

Our training framework alternates between two phases: (1) Exploration, where the model generates diverse sample trajectories via reward-guided SDE dynamics, and (2) Optimization, where model parameters are updated via GRPO.

4.3.1. SAMPLING AND EXPLORATION

Given a prompt c and shared initial noise $X_0 \sim \mathcal{N}(0, I)$, we generate G trajectories $\{X_{0:1}^i\}_{i=1}^G$. Sample diversity arises naturally from the stochastic Wiener process W_t in our SDE formulation (Equation (12)). We discretize the continuous-time dynamics via Euler-Maruyama. With step size Δt , the update rule becomes:

$$X_{k+1}^i = X_k^i + \mathcal{D}_{\text{total}}(X_k^i, t_k) \Delta t + \sqrt{2\epsilon_{t_k} \Delta t} Z_k^i, \quad (14)$$

where $Z_k^i \sim \mathcal{N}(0, I)$. The drift $\mathcal{D}_{\text{total}}$ combines the flow matching prior with the process reward gradient:

$$\mathcal{D}_{\text{total}}(X, t) = \left(1 + \frac{t\epsilon_t}{1-t}\right) u_\theta(X, t) - \frac{\epsilon_t}{1-t} X + \frac{\epsilon_t}{\beta} \nabla_x r_p(X, t) \quad (15)$$

4.3.2. OPTIMIZATION VIA GRPO

Dual Reward Integration. For policy optimization, we employ GRPO with a dual-reward formulation: a step-wise process reward $r_p(x, t)$ and a trajectory-level outcome reward $r_o(x)$. We integrate these signals by defining the total advantage at step k as the sum of their group-normalized values. Concretely, for the i -th sample:

$$A_{k,i} = \underbrace{\frac{r_p(X_k^i, t_k) - \mu_p^k}{\sigma_p^k}}_{\text{Process Advantage}} + \underbrace{\frac{r_o(X_T^i) - \mu_o}{\sigma_o}}_{\text{Outcome Advantage}}, \quad (16)$$

where μ and σ denote the mean and standard deviation computed over the sample group G .

Objective Function. We define the per-step importance weight between the current policy π_θ and the reference policy $\pi_{\theta_{\text{old}}}$ as $\omega_{k,i}(\theta) = \frac{\pi_\theta(X_{k+1}^i | X_k^i)}{\pi_{\theta_{\text{old}}}(X_{k+1}^i | X_k^i)}$. The GRPO objective is then formulated using the total advantage $A_{k,i}$:

$$\mathcal{L}_{\text{GRPO}}(\theta) = -\frac{1}{G} \sum_{i=1}^G \frac{1}{T} \sum_{k=0}^{T-1} \min \left(\omega_{k,i}(\theta) A_{k,i}, \text{clip}(\omega_{k,i}(\theta), 1 - \epsilon_{\text{clip}}, 1 + \epsilon_{\text{clip}}) A_{k,i} \right). \quad (17)$$

The procedure is summarized in Algorithm 1. Derivations log-probability used for $\omega_{k,i}(\theta)$ appear in Section 4.4.

4.4. Distillation for Reward-Gradient-Free Inference

The reward gradient $\frac{\epsilon_t}{\beta} \nabla_x r_p$ is applied *exclusively* during the training phase. Once training is complete, the optimized network u_θ generates samples via standard flow dynamics, *without* computing $\nabla_x r_p$. This design choice is motivated by practical considerations: retaining the reward gradient would necessitate concurrently loading the PRM alongside the video generator, increasing memory footprint and system complexity. However, this raises a natural concern regarding the distribution shift between the guided dynamics used during training and the unguided dynamics used for final inference.

To address this, we introduce a Policy Distillation formulation that explicitly internalizes the reward guidance into the flow network. We treat the reward-guided trajectory generation as a “teacher” process and optimize the “student” flow network to replicate this guided behavior without explicit reward computation. During the exploration phase of

Algorithm 1 RGG Sampling & Distillation Training

```

1: Input: Pre-trained  $u_\theta$ , PRM  $r_p$ , ORM  $r_o$ 
2: for iteration = 1, ...,  $M$  do
3:    $\theta_{\text{old}} \leftarrow \theta$ 
4:   // Phase 1: Guided Exploration
5:   for each prompt  $c, i \in \{1..G\}$  do
6:     for  $k = 0$  to  $T - 1$  do
7:        $\mathcal{D}_{\text{flow}} \leftarrow \text{FlowDrift}(X_k^i; \theta_{\text{old}})$ 
8:        $\mathcal{D}_{\text{total}} \leftarrow \mathcal{D}_{\text{flow}} + \frac{\epsilon_t}{\beta} \nabla_x r_p(X_k^i)$ 
9:        $X_{k+1}^i \leftarrow \text{Step}(X_k^i, \mathcal{D}_{\text{total}})$ 
10:       $\mu_{\text{old}} \leftarrow X_k^i + \mathcal{D}_{\text{flow}} \Delta t$ 
11:       $\log \pi_{\text{old}} \leftarrow \log \mathcal{N}(X_{k+1}^i | \mu_{\text{old}}, \sigma_t^2)$ 
12:      Store  $(X_k^i, X_{k+1}^i, \log \pi_{\text{old}}, r_p(X_k^i))$ 
13:   end for
14:   Compute  $A_k^i$  using standardized  $r_p, r_o$ 
15: end for
16: // Phase 2: Optimization
17: for minibatch  $b \in \mathcal{B}$  do
18:    $\mu_\theta \leftarrow X_k + \text{FlowDrift}(X_k; \theta) \Delta t$ 
19:    $\log \pi_\theta \leftarrow \log \mathcal{N}(X_{k+1} | \mu_\theta, \sigma_t^2)$ 
20:    $\omega \leftarrow \exp(\log \pi_\theta - \log \pi_{\text{old}})$ 
21:   Update  $\theta$  to  $\max \mathbb{E}[\min(\omega A, \text{clip}(\omega) A)]$ 
22: end for
23: end for

```

training, trajectory steps $\{X_{k+1}^i\}$ are generated using the full guided dynamics (Equation (14)), which incorporates the reward gradient term. However, when computing the log-probability of the guided steps X_{k+1}^i , both the behavior policy $\pi_{\theta_{\text{old}}}$ and the target policy π_θ are evaluated *without* explicit reward guidance in their drifts. Denoting the policy parameters as $\psi \in \{\theta, \theta_{\text{old}}\}$, we have:

$$\mu_\psi(X_k, t_k) = X_k + \Delta t \cdot \mathcal{D}_{\text{flow}}(X_k, t_k; \psi), \quad (18)$$

where $\mathcal{D}_{\text{flow}}$ denotes the flow-only component of the drift, excluding the reward gradient term. The log-probability of generating the reward-guided step X_{k+1} under policy π_ψ is computed as (C_k is a timestep-dependent constant):

$$\log \pi_\psi(X_{k+1} | X_k) = C_k - \frac{1}{4\epsilon_{t_k} \Delta t} \|X_{k+1} - \mu_\psi(X_k, t_k)\|^2. \quad (19)$$

Since X_{k+1} is generated via reward-guided dynamics while μ_ψ excludes the reward gradient, the residual $(X_{k+1} - \mu_\psi)$ implicitly encodes the reward signal. Minimizing this residual forces the student velocity field u_θ to internalize the guidance, enabling the optimized network to steer toward high-reward regions during inference without external reward computation. We provide detailed derivations and empirical comparisons in Appendix E.

5. Experiments

5.1. Experimental Setup

Post-Training Backbone & Baselines. We empirically validate Euphonium on text-to-video tasks. We implement all methods based on the open-source HunyuanVideo (Kong et al., 2024) with 14B parameters. We compare Euphonium against the base model and other leading post-training baselines: Flow-GRPO (Liu et al., 2025b) and Dance-GRPO (Xue et al., 2025).

Reward Models. Both PRM and ORM are trained on a curated dataset emphasizing visual quality and motion fidelity. For the ORM, we train a scoring model based on InternVL3-1B (Zhu et al., 2025), optimized using the Bradley-Terry objective on pairwise preference annotations. For the PRM, we fine-tune a lightweight variant of the HunyuanVideo DiT on the same preference data to predict quality scores directly from latent states x_t , conditioned on the text prompt c and diffusion timestep t .

Datasets. To train the reward model, we curate a dataset of 200,000 video samples generated from 20,000 unique prompts. We employ a pointwise binary annotation protocol, labeling samples as positive or negative based on visual quality and motion fidelity. Training pairs are then constructed by contrasting positive and negative instances to enable preference learning. For GRPO training, we collect 10,000 prompts from DanceGRPO (Xue et al., 2025) and internal portrait-centric sources, strictly held out from the reward model training set.

Evaluation Metrics. Performance is evaluated using VBFench2 (Zheng et al., 2025b). We report the Total Score alongside all five sub-scores.

5.2. Main Results

Quantitative Analysis. Table 1 presents the quantitative performance comparison on VBFench2. Euphonium demonstrates significant improvement, achieving the highest Total Score of 54.24 and outperforming the second-best method, DanceGRPO. Notably, our method secures the top rank in four out of five dimensions: Commonsense, Controllability, Human Fidelity, and Physics. While Flow-GRPO marginally leads in Creativity, Euphonium ranks a close second, proving that our approach effectively balances diverse generation with strict adherence to physical constraints and user instructions.

Visual Comparison. Figure 2 visualizes sample frames generated by Euphonium and other methods. While baselines occasionally exhibit artifacts or fail to capture prompt details, Euphonium generates videos with higher fidelity and improved prompt adherence, corroborating the effectiveness of our approach.

5.3. Training Efficiency & Computational Overhead

A primary consideration for Reward-Gradient Guidance (RGG) is whether the additional per-step computation is justified by improved training efficiency. We analyze both the computational overhead and the convergence behavior.

Computational Cost. As reported in Table 2, computing the latent PRM gradient adds only 2.4% latency per sampling step. The memory overhead is similarly modest at 8.5%. This efficiency stems from our lightweight PRM design: operating in the compressed latent space with only 8 DiT layers, compared to the 14B-parameter generative backbone with 60 layers. The marginal overhead ensures that RGG remains practical for large-scale video generation training.

Convergence Analysis. Despite marginal per-step overhead, guided exploration significantly accelerates convergence. As illustrated in Figure 1, Euphonium demonstrates superior sample efficiency by actively steering trajectories toward high-reward regions relative to baselines. Quantitatively, Euphonium attains the peak reward **1.66**× faster than DanceGRPO. This result validates that the gains in exploration efficiency effectively amortize the additional computational cost.

5.4. Ablation Study

Impact of Active Steering. As shown in Table 3, disabling the reward gradient term $\nabla_x r_p$ (w/o Active Steering) causes a performance drop from 54.24 to 53.61. This degradation substantiates the role of actively steering trajectories toward high-reward regions, as undirected stochastic exploration alone proves insufficient for effectively navigating the sparse manifold of high-quality samples.

Effectiveness of Dual-Reward Supervision. Removing the PRM from advantage computation (w/o PRM Advantage) yields 53.95, indicating that dense step-level feedback enables finer credit assignment beyond the final outcome reward. Removing the ORM instead (w/o ORM Advantage) results in 53.59, a more substantial decline that underscores the importance of pixel-level evaluation for capturing visual fidelity and fine-grained details that the latent-space PRM may overlook. Notably, the ORM ablation exhibits a comparable performance drop to removing active steering entirely, suggesting that outcome-level supervision is critical for grounding the generation process in perceptually meaningful quality metrics.

Sensitivity Analysis of Reward-Gradient Guidance. We further investigate the hyperparameters governing the RGG mechanism: the guidance coefficient and its temporal activation window.

1) *Guidance Strength.* We investigate the guidance coef-

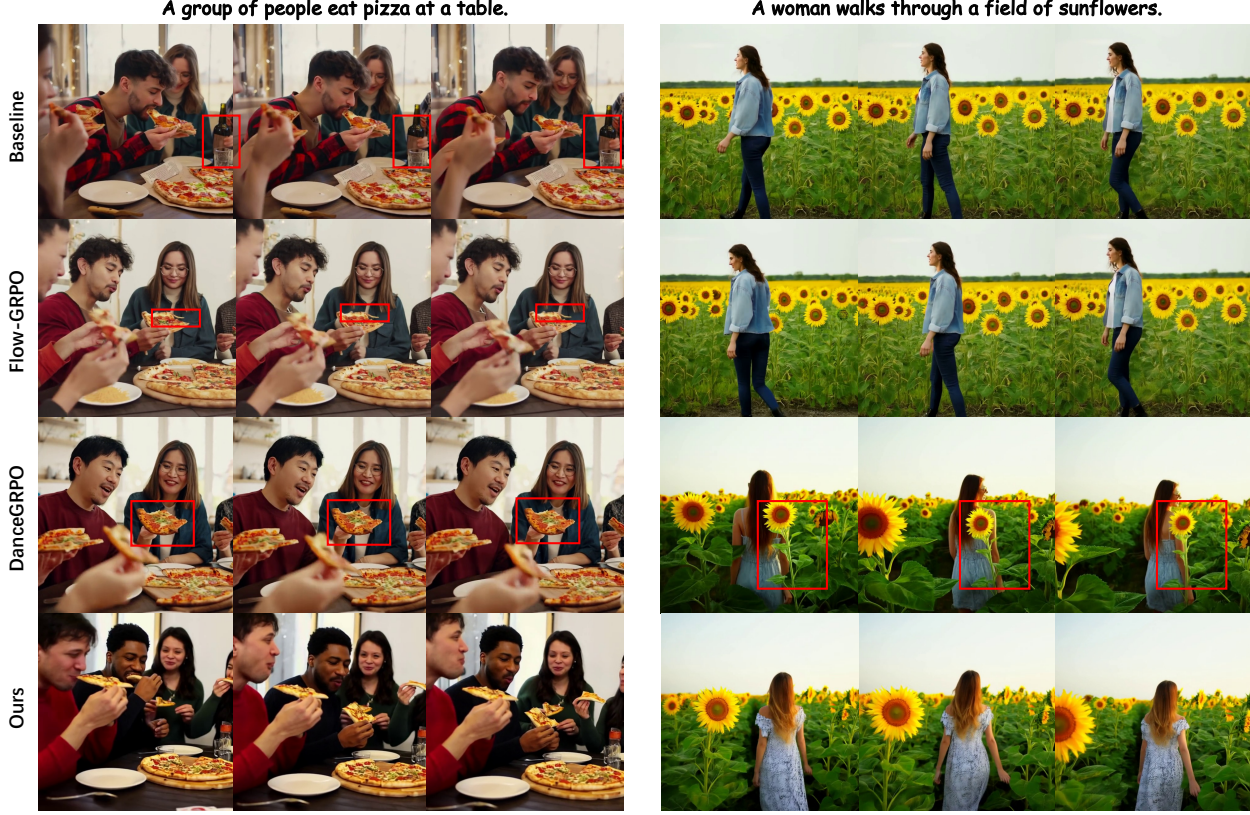


Figure 2. **Qualitative comparison.** Visual results demonstrate that Euphonium generates more coherent and prompt-aligned videos compared to the pre-trained model, Flow-GRPO and DanceGRPO.

Table 1. **Quantitative Comparison on VBench2.** The best results are highlighted in **bold**, and the second-best are underlined.

| Method | Total Score \uparrow | Creativity \uparrow | Commonsense \uparrow | Controllability \uparrow | Human Fidelity \uparrow | Physics \uparrow |
|--------------------------------|------------------------|-----------------------|------------------------|----------------------------|---------------------------|--------------------|
| Base Model (Kong et al., 2024) | 51.09 | 40.18 | <u>62.87</u> | 23.95 | 83.30 | <u>45.15</u> |
| Flow-GRPO (Liu et al., 2025b) | 51.52 | 42.42 | 62.86 | 24.41 | 85.41 | 42.48 |
| DanceGRPO (Xue et al., 2025) | <u>51.85</u> | 40.93 | 61.99 | <u>25.08</u> | <u>88.10</u> | 43.14 |
| Euphonium (Ours) | 54.24 | <u>41.42</u> | 67.17 | 26.88 | 88.91 | 46.84 |

Table 2. **RGG Overhead Analysis.** Wall-clock time and peak memory are measured on a single H800 GPU. The lightweight latent-space PRM introduces minimal overhead.

| Metric | Baseline | w/ RGG | Overhead |
|-------------------|----------|--------|----------|
| Latency (ms/step) | 1005.6 | 1030.1 | +2.4% |
| Peak VRAM (GB) | 32.9 | 35.7 | +8.5% |

ficient λ governing the RGG mechanism. We introduce a scalar coefficient $\lambda \geq 0$ to control the magnitude of reward gradient injection:

$$\mathcal{D}_{\text{total}} = \mathcal{D}_{\text{flow}} + \lambda \nabla_x r_p(X, t). \quad (20)$$

λ corresponds to ϵ_t/β in Equation (12), where β is the

Table 3. **Ablation Study.** We evaluate the impact of active steering by comparing the full Euphonium framework against variants that remove guidance or replace it with filtering strategies.

| Method Setting | VBench2 Total Score |
|-------------------------|---------------------|
| Euphonium (Full Method) | 54.24 |
| w/o Active Steering | 53.61 |
| w/o PRM Advantage | 53.95 |
| w/o ORM Advantage | 53.59 |

KL penalty. In practice, we treat λ as a tunable hyperparameter that balances alignment strength against deviation from the reference flow. As shown in Table 4, moderate guidance ($\lambda = 0.1$) yields optimal performance. Weaker guidance ($\lambda = 0.01$) provides insufficient steering toward

Table 4. Ablation on RGG Coefficient (λ). We scale the guidance gradient by a factor λ . Moderate guidance achieves the best trade-off between alignment and quality.

| Guidance Scale (λ) | VBench2 Total |
|------------------------------|---------------|
| 0.01 | 53.61 |
| 0.1 | 54.24 |
| 1.0 | 52.86 |

Table 5. Ablation on Temporal Activation. We compare different guidance windows against the unguided baseline. The results indicate that the latter-half guidance achieves the optimal balance between avoiding early-stage noise and retaining sufficient control authority for refinement.

| Guidance Window (t) | Step Range | VBench2 Total |
|--|---------------------|---------------|
| None (Baseline) | - | 53.61 |
| Full Trajectory ($0 \leq t \leq 1$) | $0 \rightarrow 16$ | 53.64 |
| Latter Half ($0.5 \leq t \leq 1$) | $8 \rightarrow 16$ | 54.24 |
| Late Stage ($0.75 \leq t \leq 1$) | $12 \rightarrow 16$ | 54.14 |

high-reward regions, while stronger guidance ($\lambda = 1.0$) causes over-correction that distorts the learned flow dynamics and degrades generation quality.

2) *Temporal Activation Window.* We investigate the temporal sensitivity of RGG across the denoising trajectory. Although the baseline already achieves a competitive score of 53.61 due to the dual-reward design, applying RGG yields further improvements. However, full-trajectory guidance provides only marginal gains. We attribute this to distinct limitations at both ends of the trajectory. Despite the PRM maintaining consistent accuracy ($> 70\%$) across all noise levels shown in Figure 3, we observe that applying guidance in the early stage ($t < 0.5$) could disturb the formation of structure and motion. This aggressive steering induces temporal incoherence, resulting in discontinuous frame transitions that negate the benefits of guidance. Conversely, while late-stage guidance ($t > 0.75$) avoids these issues, the restricted optimization window provides insufficient steps to accumulate effective corrective updates. Consequently, the latter half achieves the optimal balance, bypassing the sensitive initialization phase while retaining sufficient capacity for refinement.

5.5. Analysis of the Process Reward Model

The validity of our methodology relies on the premise that the Latent PRM provides accurate quality assessment even at intermediate noisy states. For reward-gradient guidance to be effective, the PRM must preserve reliable predictions at noisy intermediate states, not merely at clean data.

As shown in Figure 3, our Latent PRM maintains reliable accuracy ($> 70\%$) across all evaluated noise levels, with

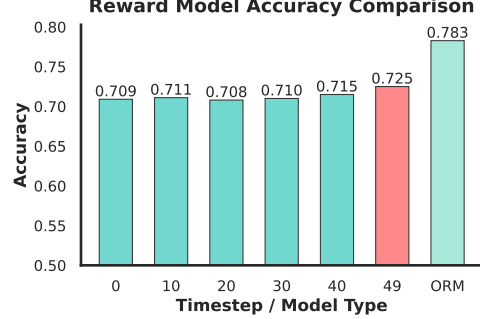


Figure 3. Accuracy of the Latent PRM. We evaluate pairwise accuracy at different timesteps against the pixel-space ORM. The PRM maintains reliable accuracy ($> 70\%$), validating its effectiveness for guiding intermediate states.

performance approaching that of the pixel-space ORM at lower noise levels. This confirms that the latent-space PRM serves as an effective proxy for visual quality assessment while operating in the latent space.

6. Conclusion

In this paper, we introduced Euphonium, a principled framework that incorporates process reward gradient guided dynamics into video flow matching for efficient post-training alignment. By deriving a reward-augmented SDE that injects dense gradient signals directly into the flow drift, our method enables active steering toward high-reward regions during exploration, theoretically encompassing prior sampling strategies as special cases. We further proposed a distillation objective that internalizes the guidance signal into the flow network, eliminating inference-time dependency on the reward model. Combined with our dual-reward optimization scheme, Euphonium achieves better alignment compared to existing methods while accelerating training convergence by **1.66 \times** .

Limitations & Future Work. Our framework relies on a Latent PRM, which presents two constraints. First, research on latent-space PRMs for video remains in an early stage, and their robustness compared to pixel-based models requires further investigation. Second, the PRM is tightly coupled with the specific VAE latent space of the generative backbone, limiting transferability across different video generation architectures. Future research could explore Representation Autoencoders (RAE) (Zheng et al., 2025a), which utilize fixed, pre-trained visual encoders (e.g., DINOv2) to define a shared latent space. This offers a promising direction for developing universal, backbone-agnostic PRMs that generalize across video generation models without architecture-specific retraining.

Impact Statement

This paper presents work whose goal is to advance the field of Machine Learning. There are many potential societal consequences of our work, none which we feel must be specifically highlighted here.

References

Albergo, M. S. and Vanden-Eijnden, E. Nets: A non-equilibrium transport sampler. *arXiv preprint arXiv:2410.02711*, 2024.

Albergo, M. S., Boffi, N. M., and Vanden-Eijnden, E. Stochastic interpolants: A unifying framework for flows and diffusions. *arXiv preprint arXiv:2303.08797*, 2023.

Black, K., Janner, M., Du, Y., Kostrikov, I., and Levine, S. Training diffusion models with reinforcement learning. *arXiv preprint arXiv:2305.13301*, 2023.

Bradley, R. A. and Terry, M. E. Rank analysis of incomplete block designs: I. the method of paired comparisons. *Biometrika*, 39(3/4):324–345, 1952.

DeepMind, G. Veo 3. <https://deepmind.google/models/veo>, 2025.

Ding, Z. and Ye, W. Treegrpo: Tree-advantage grpo for online rl post-training of diffusion models. *arXiv preprint arXiv:2512.08153*, 2025.

Esser, P., Kulal, S., Blattmann, A., Entezari, R., Müller, J., Saini, H., Levi, Y., Lorenz, D., Sauer, A., Boesel, F., et al. Scaling rectified flow transformers for high-resolution image synthesis. In *Forty-first international conference on machine learning*, 2024.

Gao, Y., Guo, H., Hoang, T., Huang, W., Jiang, L., Kong, F., Li, H., Li, J., Li, L., Li, X., et al. Seedance 1.0: Exploring the boundaries of video generation models. *arXiv preprint arXiv:2506.09113*, 2025.

He, X., Fu, S., Zhao, Y., Li, W., Yang, J., Yin, D., Rao, F., and Zhang, B. Tempflow-grpo: When timing matters for grpo in flow models. *arXiv preprint arXiv:2508.04324*, 2025.

Ho, J. and Salimans, T. Classifier-free diffusion guidance. *arXiv preprint arXiv:2207.12598*, 2022.

Kong, W., Tian, Q., Zhang, Z., Min, R., Dai, Z., Zhou, J., Xiong, J., Li, X., Wu, B., Zhang, J., et al. Hunyuan-video: A systematic framework for large video generative models. *arXiv preprint arXiv:2412.03603*, 2024.

Li, J., Cui, Y., Huang, T., Ma, Y., Fan, C., Yang, M., and Zhong, Z. Mixgrpo: Unlocking flow-based grpo efficiency with mixed ode-sde. *arXiv preprint arXiv:2507.21802*, 2025.

Lightman, H., Kosaraju, V., Burda, Y., Edwards, H., Baker, B., Lee, T., Leike, J., Schulman, J., Sutskever, I., and Cobbe, K. Let’s verify step by step. In *The Twelfth International Conference on Learning Representations*, 2023.

Lipman, Y., Chen, R. T., Ben-Hamu, H., Nickel, M., and Le, M. Flow matching for generative modeling. *arXiv preprint arXiv:2210.02747*, 2022.

Liu, F., Wang, H., Cai, Y., Zhang, K., Zhan, X., and Duan, Y. Video-t1: Test-time scaling for video generation. *arXiv preprint arXiv:2503.18942*, 2025a.

Liu, J., Liu, G., Liang, J., Li, Y., Liu, J., Wang, X., Wan, P., Zhang, D., and Ouyang, W. Flow-grpo: Training flow matching models via online rl. *arXiv preprint arXiv:2505.05470*, 2025b.

Liu, J., Liu, G., Liang, J., Yuan, Z., Liu, X., Zheng, M., Wu, X., Wang, Q., Xia, M., Wang, X., et al. Improving video generation with human feedback. *arXiv preprint arXiv:2501.13918*, 2025c.

Liu, X., Gong, C., and Liu, Q. Flow straight and fast: Learning to generate and transfer data with rectified flow. *arXiv preprint arXiv:2209.03003*, 2022.

Liu, Z., Xiao, T. Z., Domingo-Enrich, C., Liu, W., and Zhang, D. Value gradient guidance for flow matching alignment. *arXiv preprint arXiv:2512.05116*, 2025d.

Loshchilov, I. and Hutter, F. Decoupled weight decay regularization. *arXiv preprint arXiv:1711.05101*, 2017.

Lu, C., Chen, H., Chen, J., Su, H., Li, C., and Zhu, J. Contrastive energy prediction for exact energy-guided diffusion sampling in offline reinforcement learning. In *International Conference on Machine Learning*, pp. 22825–22855. PMLR, 2023.

Luo, Y., Du, P., Li, B., Du, S., Zhang, T., Chang, Y., Wu, K., Gai, K., and Wang, X. Sample by step, optimize by chunk: Chunk-level grpo for text-to-image generation. *arXiv preprint arXiv:2510.21583*, 2025.

Mi, X., Yu, W., Lian, J., Jie, S., Zhong, R., Liu, Z., Zhang, G., Zhou, Z., Xu, Z., Zhou, Y., et al. Video generation models are good latent reward models. *arXiv preprint arXiv:2511.21541*, 2025.

OpenAI. Sora 2. <https://openai.com/sora>, 2025.

Paszke, A., Gross, S., Massa, F., Lerer, A., Bradbury, J., Chanan, G., Killeen, T., Lin, Z., Gimelshein, N., Antiga, L., et al. Pytorch: An imperative style, high-performance deep learning library. *Advances in neural information processing systems*, 32, 2019.

Rafailov, R., Sharma, A., Mitchell, E., Manning, C. D., Ermon, S., and Finn, C. Direct preference optimization: Your language model is secretly a reward model. *Advances in neural information processing systems*, 36: 53728–53741, 2023.

Technology, K. Kling. <https://klingai.com/global>, 2025.

Tong, A., Fatras, K., Malkin, N., Huguet, G., Zhang, Y., Rector-Brooks, J., Wolf, G., and Bengio, Y. Improving and generalizing flow-based generative models with mini-batch optimal transport. *arXiv preprint arXiv:2302.00482*, 2023.

Wan, T., Wang, A., Ai, B., Wen, B., Mao, C., Xie, C.-W., Chen, D., Yu, F., Zhao, H., Yang, J., et al. Wan: Open and advanced large-scale video generative models. *arXiv preprint arXiv:2503.20314*, 2025.

Xu, J., Liu, X., Wu, Y., Tong, Y., Li, Q., Ding, M., Tang, J., and Dong, Y. Imagereward: Learning and evaluating human preferences for text-to-image generation. *Advances in Neural Information Processing Systems*, 36: 15903–15935, 2023.

Xue, Z., Wu, J., Gao, Y., Kong, F., Zhu, L., Chen, M., Liu, Z., Liu, W., Guo, Q., Huang, W., et al. Dancegrpo: Unleashing grpo on visual generation. *arXiv preprint arXiv:2505.07818*, 2025.

Zhang, S., Zhang, Z., Dai, C., and Duan, Y. E-grpo: High entropy steps drive effective reinforcement learning for flow models. *arXiv preprint arXiv:2601.00423*, 2026.

Zhao, Y., Gu, A., Varma, R., Luo, L., Huang, C.-C., Xu, M., Wright, L., Shojanazeri, H., Ott, M., Shleifer, S., et al. Pytorch fsdp: experiences on scaling fully sharded data parallel. *arXiv preprint arXiv:2304.11277*, 2023.

Zheng, B., Ma, N., Tong, S., and Xie, S. Diffusion transformers with representation autoencoders. *arXiv preprint arXiv:2510.11690*, 2025a.

Zheng, D., Huang, Z., Liu, H., Zou, K., He, Y., Zhang, F., Gu, L., Zhang, Y., He, J., Zheng, W.-S., et al. Vbench-2.0: Advancing video generation benchmark suite for intrinsic faithfulness. *arXiv preprint arXiv:2503.21755*, 2025b.

Zheng, Q., Le, M., Shaul, N., Lipman, Y., Grover, A., and Chen, R. T. Guided flows for generative modeling and decision making. *arXiv preprint arXiv:2311.13443*, 2023.

Zhu, J., Wang, W., Chen, Z., Liu, Z., Ye, S., Gu, L., Tian, H., Duan, Y., Su, W., Shao, J., et al. Internvl3: Exploring advanced training and test-time recipes for open-source multimodal models. *arXiv preprint arXiv:2504.10479*, 2025.

Appendix

- Appendix A presents the formal proof of Proposition 3.1, establishing the mathematical relationship between the marginal score function and the optimal velocity field under the Linear Optimal Transport path.
- Appendix B demonstrates that our derived stochastic dynamics naturally recover the sampling procedure proposed in Flow-GRPO, thereby establishing the theoretical foundation underlying these recent methods.
- Appendix C provides the complete derivation of the optimal policy that maximizes expected reward subject to a KL divergence constraint, using the method of Lagrange multipliers.
- Appendix D justifies our design choice of constructing a dedicated Process Reward Model in the latent space, analyzing the computational infeasibility of alternative approaches including decoder backpropagation and zeroth-order gradient estimation.
- Appendix E details the derivation of policy log-probability objectives used in our GRPO formulation, presenting both the standard optimization setting and the policy distillation variant that enables gradient-free inference. This section also includes an empirical comparison of different inference protocols.
- Appendix F provides comprehensive implementation details, including hyperparameter configurations, training infrastructure, and sampling settings used throughout our experiments.

A. Proof of Score-Velocity Relationship (Proposition 3.1)

In this section, we provide the derivation for the relationship between the marginal score function $\nabla \log p_t(x)$ and the optimal vector field $u_t(x)$ under the Linear Optimal Transport (OT) path (Zheng et al., 2023).

Setup. Consider the linear interpolation path defined as:

$$X_t = (1-t)X_0 + tX_1, \quad (21)$$

where the source distribution is standard Gaussian, $X_0 \sim p_0 = \mathcal{N}(0, I)$, and $X_1 \sim p_{\text{data}}$.

1. Derivation of the Optimal Vector Field $u_t(x)$. The optimal vector field $u_t(x)$ that generates the probability path p_t minimizes the flow matching objective. It is known to be the expected instantaneous velocity conditioned on the current location $X_t = x$:

$$u_t(x) = \mathbb{E} \left[\frac{d}{dt} X_t \mid X_t = x \right]. \quad (22)$$

Taking the time derivative of the path yields $\dot{X}_t = X_1 - X_0$. We can express X_0 in terms of X_t and X_1 as:

$$X_0 = \frac{X_t - tX_1}{1-t}. \quad (23)$$

Substituting this back into the velocity expression:

$$\dot{X}_t = X_1 - \frac{X_t - tX_1}{1-t} = \frac{(1-t)X_1 - X_t + tX_1}{1-t} = \frac{X_1 - X_t}{1-t}. \quad (24)$$

Thus, the conditional vector field is:

$$u_t(x) = \frac{\mathbb{E}[X_1 \mid X_t = x] - x}{1-t}. \quad (25)$$

2. Derivation of the Marginal Score $\nabla \log p_t(x)$. Conditioned on a fixed data point $X_1 = x_1$, the variable X_t follows a Gaussian distribution because X_0 is Gaussian:

$$p(x_t \mid x_1) = \mathcal{N}(x_t; tx_1, (1-t)^2 I). \quad (26)$$

The score of this conditional density is:

$$\nabla_{x_t} \log p(x_t \mid x_1) = -\frac{x_t - tx_1}{(1-t)^2}. \quad (27)$$

Using the identity $\nabla \log p_t(x) = \mathbb{E}_{X_1|X_t=x}[\nabla_x \log p(x | X_1)]$, we have:

$$\begin{aligned}\nabla \log p_t(x) &= \mathbb{E} \left[-\frac{x - tX_1}{(1-t)^2} \middle| X_t = x \right] \\ &= -\frac{1}{(1-t)^2} (x - t\mathbb{E}[X_1 | X_t = x]).\end{aligned}\tag{28}$$

Rearranging for the conditional expectation:

$$\mathbb{E}[X_1 | X_t = x] = \frac{1}{t} (x + (1-t)^2 \nabla \log p_t(x)).\tag{29}$$

Note that Equation (29) is essentially Tweedie's formula adapted for the linear OT path.

3. Connecting Score and Velocity. We substitute the term $\mathbb{E}[X_1 | X_t = x]$ from Equation (25) into the score equation. From Equation (25), we have:

$$\mathbb{E}[X_1 | X_t = x] = x + (1-t)u_t(x).\tag{30}$$

Substitute this into the score expression:

$$\begin{aligned}\nabla \log p_t(x) &= -\frac{1}{(1-t)^2} (x - t[x + (1-t)u_t(x)]) \\ &= -\frac{1}{(1-t)^2} (x - tx - t(1-t)u_t(x)) \\ &= -\frac{1}{(1-t)^2} ((1-t)x - t(1-t)u_t(x)) \\ &= -\frac{1}{1-t} (x - tu_t(x)).\end{aligned}\tag{31}$$

□

B. Equivalence to Flow-GRPO Dynamics

In this appendix, we demonstrate that the specific stochastic dynamics derived in Equation (7) naturally recover the dynamics proposed in recent works such as Flow-GRPO. By showing this mathematical alignment, we establish that our framework provides the underlying mathematical foundation for these sampling methods.

Notation Mapping. We distinguish between the variables used in our framework and those in Flow-GRPO as follows:

- **Time Convention:** Flow-GRPO defines time $\tau \in [0, 1]$ (reverse process, $\tau = 0$ is data). In our settings, we define time $t \in [0, 1]$ (forward process, $t = 1$ is data). The relationship is:

$$t = 1 - \tau, \quad dt = -d\tau.\tag{32}$$

- **State Variable:** Let x_τ denote the state in Flow-GRPO at time τ , and X_t denote the state in our framework at time t . Since they represent the same physical trajectory viewed from different temporal directions, the correspondence is:

$$X_{1-\tau} \equiv x_\tau.\tag{33}$$

- **Velocity Field:** Let $v_\tau(x_\tau)$ be the velocity in Flow-GRPO (pointing data \rightarrow noise). Our velocity $u_t(X_t)$ points noise \rightarrow data. At the corresponding physical state, these vectors are opposite:

$$u_{1-\tau}(X_{1-\tau}) = -v_\tau(x_\tau).\tag{34}$$

- **Noise Level:** Flow-GRPO uses diffusion coefficient σ_τ . Mapping this to our noise schedule ϵ_t at the equivalent time $t = 1 - \tau$:

$$\epsilon_{1-\tau} = \frac{1}{2} \sigma_\tau^2.\tag{35}$$

Derivation. The Flow-GRPO SDE for generation is given by:

$$dx_\tau = \left[v_\tau(x_\tau) + \frac{\sigma_\tau^2}{2\tau} (x_\tau + (1 - \tau)v_\tau(x_\tau)) \right] d\tau + \sigma_\tau dw. \quad (36)$$

To prove equivalence, we start with our derived drift term \mathcal{D}_t for the state X_t :

$$\mathcal{D}_t = \left(1 + \frac{t\epsilon_t}{1-t} \right) u_t(X_t) - \frac{\epsilon_t}{1-t} X_t. \quad (37)$$

We proceed step-by-step. First, we substitute the time variable $t = 1 - \tau$ into our expression, while keeping the function forms generic:

$$\begin{aligned} \mathcal{D}_{1-\tau} &= \left(1 + \frac{(1-\tau)\epsilon_{1-\tau}}{1-(1-\tau)} \right) u_{1-\tau}(X_{1-\tau}) - \frac{\epsilon_{1-\tau}}{1-(1-\tau)} X_{1-\tau} \\ &= \left(1 + \frac{(1-\tau)\epsilon_{1-\tau}}{\tau} \right) u_{1-\tau}(X_{1-\tau}) - \frac{\epsilon_{1-\tau}}{\tau} X_{1-\tau}. \end{aligned} \quad (38)$$

Next, we apply the notation mappings: $X_{1-\tau} \rightarrow x_\tau$, $u_{1-\tau}(X_{1-\tau}) \rightarrow -v_\tau(x_\tau)$, and $\epsilon_{1-\tau} \rightarrow \sigma_\tau^2/2$:

$$\begin{aligned} \mathcal{D}_{1-\tau} &= \left(1 + \frac{(1-\tau)(\sigma_\tau^2/2)}{\tau} \right) (-v_\tau(x_\tau)) - \frac{\sigma_\tau^2/2}{\tau} x_\tau \\ &= -v_\tau(x_\tau) - \frac{(1-\tau)\sigma_\tau^2}{2\tau} v_\tau(x_\tau) - \frac{\sigma_\tau^2}{2\tau} x_\tau \\ &= - \left[v_\tau(x_\tau) + \frac{\sigma_\tau^2}{2\tau} (x_\tau + (1-\tau)v_\tau(x_\tau)) \right]. \end{aligned} \quad (39)$$

Finally, considering the differential time relation $dt = -d\tau$, the infinitesimal update in our framework becomes:

$$dX_t = \mathcal{D}_t dt = \mathcal{D}_{1-\tau}(-d\tau) = \left[v_\tau(x_\tau) + \frac{\sigma_\tau^2}{2\tau} (x_\tau + (1-\tau)v_\tau(x_\tau)) \right] d\tau. \quad (40)$$

This matches the drift term of the Flow-GRPO SDE exactly, confirming that both frameworks describe the same underlying stochastic process.

C. Derivation of the Optimal Policy

In this section, we provide the formal derivation for the optimal policy π^* that maximizes the expected reward subject to a KL divergence constraint. Following the framework of Direct Preference Optimization (DPO) (Rafailov et al., 2023), we employ the method of Lagrange multipliers to solve for the optimal distribution directly without assuming a candidate form.

Problem Statement. We aim to determine a policy $\pi(x)$ that maximizes the following objective functional:

$$\mathcal{J}(\pi) = \mathbb{E}_{x \sim \pi}[r(x)] - \beta D_{\text{KL}}(\pi \| \pi_{\text{ref}}) = \int \pi(x) r(x) dx - \beta \int \pi(x) \log \frac{\pi(x)}{\pi_{\text{ref}}(x)} dx, \quad (41)$$

subject to the normalization constraint ensuring $\pi(x)$ is a valid probability density function:

$$\mathcal{C}(\pi) = \int \pi(x) dx - 1 = 0. \quad (42)$$

Derivation. We construct the Lagrangian functional $\mathcal{L}(\pi, \lambda)$, where λ is the Lagrange multiplier associated with the normalization constraint:

$$\mathcal{L}(\pi, \lambda) = \mathcal{J}(\pi) - \lambda \left(\int \pi(x) dx - 1 \right). \quad (43)$$

Expanding the terms, we have:

$$\mathcal{L}(\pi, \lambda) = \int \pi(x) (r(x) - \beta \log \pi(x) + \beta \log \pi_{\text{ref}}(x) - \lambda) dx + \lambda. \quad (44)$$

To find the stationary point π^* , we take the functional derivative of \mathcal{L} with respect to $\pi(x)$ and set it to zero (the Euler-Lagrange condition):

$$\frac{\delta \mathcal{L}}{\delta \pi(x)} = r(x) - \beta(1 + \log \pi(x)) + \beta \log \pi_{\text{ref}}(x) - \lambda = 0. \quad (45)$$

Note that $\frac{\delta}{\delta \pi}(\pi \log \pi) = 1 + \log \pi$. Rearranging the terms to solve for $\log \pi(x)$:

$$\beta \log \pi(x) = r(x) + \beta \log \pi_{\text{ref}}(x) - (\beta + \lambda). \quad (46)$$

Dividing by β and exponentiating both sides, we obtain the general form of the optimal policy:

$$\pi^*(x) = \pi_{\text{ref}}(x) \exp\left(\frac{r(x)}{\beta}\right) \exp\left(-1 - \frac{\lambda}{\beta}\right). \quad (47)$$

The term $\exp\left(-1 - \frac{\lambda}{\beta}\right)$ is independent of x and serves as the normalization constant. Let $Z^{-1} = \exp\left(-1 - \frac{\lambda}{\beta}\right)$. Using the constraint $\int \pi^*(x) dx = 1$, we determine Z :

$$\int \frac{1}{Z} \pi_{\text{ref}}(x) \exp\left(\frac{r(x)}{\beta}\right) dx = 1 \implies Z = \int \pi_{\text{ref}}(x) \exp\left(\frac{r(x)}{\beta}\right) dx. \quad (48)$$

Thus, the optimal policy is uniquely determined as:

$$\pi^*(x) = \frac{1}{Z} \pi_{\text{ref}}(x) \exp\left(\frac{r(x)}{\beta}\right). \quad (49)$$

□

D. Justification for Latent-Space Guidance

In Section 4.2, we construct a dedicated PRM operating in the latent space. While utilizing off-the-shelf pixel-space reward models (e.g., VideoAlign (Liu et al., 2025c)) is theoretically appealing, it presents significant computational challenges for online optimization. We analyze two alternative integration strategies and detail why both are impractical for our framework: direct backpropagation via the decoder and zeroth-order gradient estimation.

D.1. Memory Constraints of Decoder Backpropagation

A direct approach to guide the latent x_t is to chain the generation and scoring processes. Based on the Linear Optimal Transport path defined in Section 3, the clean latent \hat{x}_1 can be estimated from the current noisy state x_t via the vector field u_θ :

$$\hat{x}_1 = x_t + (1 - t)u_\theta(x_t, t). \quad (50)$$

Let $\hat{v} = \mathcal{D}(\hat{x}_1)$ denote the decoded video pixels. The gradient of the reward $s = r_{\text{pixel}}(\hat{v})$ with respect to x_t is given by the chain rule:

$$\nabla_{x_t} s = \underbrace{\left(\frac{\partial \hat{x}_1}{\partial x_t}\right)^\top}_{\text{Denoise Grad}} \cdot \underbrace{\left(\frac{\partial \mathcal{D}}{\partial \hat{x}_1}\right)^\top}_{\text{Decoder Jacobian}} \cdot \underbrace{\nabla_{\hat{v}} r_{\text{pixel}}}_{\text{Reward Grad}} \quad (51)$$

The bottleneck lies in the Decoder Jacobian term. Video VAEs employ high spatial-temporal compression ratios (e.g., $8 \times 8 \times 4$), resulting in pixel-space tensors \hat{v} that are orders of magnitude larger than the latent x_t . Backpropagating through the decoder requires storing dense activation maps for the entire video sequence, which exceeds the VRAM capacity of typical training GPUs and causes Out-Of-Memory errors.

D.2. Variance Issues in Zeroth-Order Estimation

To circumvent memory constraints, one might employ zeroth-order (derivative-free) optimization such as Simultaneous Perturbation Stochastic Approximation (SPSA), which estimates gradients using only forward passes without storing activation graphs.

For a composite reward function $F(x_t) = r_{\text{pixel}}(\mathcal{D}(\text{denoise}(x_t)))$, the gradient can be approximated via two-sided perturbation with a random vector $z \sim \mathcal{N}(0, I)$:

$$\hat{g}_{\text{SPSA}}(x_t) \approx \frac{F(x_t + \sigma z) - F(x_t - \sigma z)}{2\sigma} z, \quad (52)$$

where σ is the perturbation scale. While memory-efficient, this estimator suffers from high variance in high-dimensional latent spaces. Obtaining a reliable descent direction typically requires averaging over K independent perturbations, where larger K reduces variance but proportionally increases computational cost.

In our experiments, we attempted gradient estimation with minimal sampling ($K = 1$), using a single sample perturbed twice to obtain positive and negative variants. The resulting videos exhibited severe degradation, with visual content collapsing into block-shaped noise patterns. This failure mode indicates that single-sample SPSA provides insufficient gradient signal for meaningful optimization in high-dimensional video latent spaces. Increasing K to achieve acceptable variance (e.g., $K \geq 10$) would require decoding and scoring dozens of video candidates at every timestep, introducing prohibitive latency.

D.3. Summary

Given that backpropagation is strictly memory-bound and accurate zeroth-order estimation is time-bound, training a dedicated PRM directly in the latent space offers the necessary balance between gradient quality and computational efficiency.

E. Derivation of Policy Log-Probability Objectives

In this section, we provide the detailed derivation of the log-probability $\log \pi_{\theta}(X_{k+1}^i | X_k^i)$ used to compute the importance sampling ratio $\omega_{k,i}(\theta)$ in the GRPO objective. We present two formulations corresponding to different inference requirements after training: (1) Standard Optimization, where reward gradients are explicitly used during both training and inference; and (2) Policy Distillation, where the reward guidance is distilled into the flow network.

E.1. Standard Gradient-Guided Optimization

We first derive the objective for the standard setting. In this setting, both the behavior policy used for sampling and the target policy being optimized are defined to explicitly incorporate the Reward-Gradient Guidance (RGG).

Let ψ denote the policy parameters (where $\psi \in \{\theta, \theta_{\text{old}}\}$). The transition mean $\mu_{\psi}(X_k, t_k)$ from state X_k to X_{k+1} is defined as the current state plus the total drift:

$$\mu_{\psi}(X_k, t_k) = X_k + \Delta t \cdot \mathcal{D}_{\text{total}}(X_k, t_k; \psi). \quad (53)$$

The total drift $\mathcal{D}_{\text{total}}$ consists of the learnable flow field and the fixed reward guidance:

$$\mathcal{D}_{\text{total}}(X, t; \psi) = \underbrace{\left[\left(1 + \frac{t\epsilon_t}{1-t} \right) u_{\psi}(X, t) - \frac{\epsilon_t}{1-t} X \right]}_{\text{Flow Drift } \mathcal{D}_{\text{flow}}} + \underbrace{\frac{\epsilon_t}{\beta} \nabla_x r_p(X, t)}_{\text{Reward Guidance}}. \quad (54)$$

Phase 1: Sampling (Data Collection). During exploration, we generate trajectories using the frozen behavior policy θ_{old} . The next state X_{k+1} is sampled via:

$$X_{k+1} = \mu_{\theta_{\text{old}}}(X_k, t_k) + \sqrt{2\epsilon_{t_k} \Delta t} Z_k, \quad (55)$$

where $Z_k \sim \mathcal{N}(0, I)$ is standard Gaussian noise. The log-probability of generating this specific sample is (C_k is a timestep-dependent constant):

$$\begin{aligned} \log \pi_{\theta_{\text{old}}}(X_{k+1} | X_k) &= C_k - \frac{1}{4\epsilon_{t_k} \Delta t} \|X_{k+1} - \mu_{\theta_{\text{old}}}(X_k, t_k)\|^2 \\ &= C_k - \frac{1}{4\epsilon_{t_k} \Delta t} \left\| \sqrt{2\epsilon_{t_k} \Delta t} Z_k \right\|^2 \\ &= C_k - \frac{1}{2} \|Z_k\|^2. \end{aligned} \quad (56)$$

Phase 2: Optimization Objective. During the GRPO update, we maximize the log-probability of the target policy π_θ generating the sample X_{k+1} . The log-probability is given by:

$$\log \pi_\theta(X_{k+1}|X_k) = C_k - \frac{1}{4\epsilon_{t_k}\Delta t} \|X_{k+1} - \mu_\theta(X_k, t_k)\|^2. \quad (57)$$

Substituting Equation (55) into the residual $(X_{k+1} - \mu_\theta)$ and expanding the drift definitions reveals that the reward guidance terms cancel out:

$$\begin{aligned} X_{k+1} - \mu_\theta(X_k, t_k) &= \left(\mu_{\theta_{\text{old}}}(X_k, t_k) + \sqrt{2\epsilon_{t_k}\Delta t} Z_k \right) - \mu_\theta(X_k, t_k) \\ &= \sqrt{2\epsilon_{t_k}\Delta t} Z_k + (\mu_{\theta_{\text{old}}}(X_k, t_k) - \mu_\theta(X_k, t_k)) \\ &= \sqrt{2\epsilon_{t_k}\Delta t} Z_k + \Delta t (\mathcal{D}_{\text{total}}(X_k; \theta_{\text{old}}) - \mathcal{D}_{\text{total}}(X_k; \theta)) \\ &= \sqrt{2\epsilon_{t_k}\Delta t} Z_k + \Delta t \left(\left[\mathcal{D}_{\text{flow}}^{\text{old}} + \frac{\epsilon}{\beta} \nabla_x r_p \right] - \left[\mathcal{D}_{\text{flow}}^\theta + \frac{\epsilon}{\beta} \nabla_x r_p \right] \right) \\ &= \sqrt{2\epsilon_{t_k}\Delta t} Z_k + \Delta t \left(\left[\left(1 + \frac{t\epsilon}{1-t} \right) u_{\theta_{\text{old}}} - \frac{\epsilon}{1-t} X_k \right] - \left[\left(1 + \frac{t\epsilon}{1-t} \right) u_\theta - \frac{\epsilon}{1-t} X_k \right] \right) \\ &= \sqrt{2\epsilon_{t_k}\Delta t} Z_k + \Delta t \left(1 + \frac{t_k\epsilon_{t_k}}{1-t_k} \right) (u_{\theta_{\text{old}}}(X_k, t_k) - u_\theta(X_k, t_k)). \end{aligned} \quad (58)$$

Remark on Inference/Deployment. From a theoretical standpoint, the SDE formulation implies that the reward gradient $\nabla_x r_p$ constitutes an intrinsic component of the drift, suggesting it should be retained during inference to strictly match the training dynamics. However, retaining this term for deployment introduces a significant practical bottleneck: it necessitates the concurrent deployment of the auxiliary PRM alongside the video generator, increasing system complexity and memory footprint. Empirically, we observe that through the GRPO optimization process, the flow network u_θ implicitly learns to approximate the guided field. Consequently, for standard deployment (which we term the Implicit Mode), we can discard the external reward gradient and rely solely on the learned weights of u_θ . This strategy eliminates the dependency on the external LRM while maintaining high alignment performance.

E.2. Policy Distillation for Gradient-Free Inference

We now consider the Policy Distillation scenario. In this formulation, we treat the reward-guided trajectory generation as a “teacher” process and optimize the “student” flow network to internalize this guidance, enabling gradient-free inference.

Teacher Process (Data Collection & Distribution Shift). First, we analyze the behavior of the teacher model. We generate trajectories using the explicitly guided behavior policy, but we evaluate the sample’s probability under the *unguided* behavior policy to quantify the distribution shift induced by the reward.

The unguided teacher mean $\mu_{\theta_{\text{old}}}$ is defined purely by the base flow dynamics:

$$\mu_{\theta_{\text{old}}}(X_k, t_k) = X_k + \Delta t \cdot \mathcal{D}_{\text{flow}}(X_k, t_k; \theta_{\text{old}}). \quad (59)$$

However, the sample X_{k+1} is generated using the Guided Dynamics:

$$X_{k+1} = X_k + \Delta t \left[\mathcal{D}_{\text{flow}}(X_k, t_k; \theta_{\text{old}}) + \frac{\epsilon_{t_k}}{\beta} \nabla_x r_p(X_k, t_k) \right] + \sqrt{2\epsilon_{t_k}\Delta t} Z_k. \quad (60)$$

We derive the log-probability of this guided sample under the unguided teacher policy:

$$\log \pi_{\theta_{\text{old}}}(X_{k+1}|X_k) = C_k - \frac{1}{4\epsilon_{t_k}\Delta t} \|X_{k+1} - \mu_{\theta_{\text{old}}}(X_k, t_k)\|^2. \quad (61)$$

Substituting Equation (60) into the residual term, we observe the explicit shift:

$$\begin{aligned} X_{k+1} - \mu_{\theta_{\text{old}}}(X_k, t_k) &= \left(X_k + \Delta t \left[\mathcal{D}_{\text{flow}}^{\text{old}} + \frac{\epsilon_{t_k}}{\beta} \nabla_x r_p \right] + \sqrt{2\epsilon_{t_k}\Delta t} Z_k \right) - (X_k + \Delta t \mathcal{D}_{\text{flow}}^{\text{old}}) \\ &= \sqrt{2\epsilon_{t_k}\Delta t} Z_k + \Delta t \left(\mathcal{D}_{\text{flow}}(X_k, t_k; \theta_{\text{old}}) - \mathcal{D}_{\text{flow}}(X_k, t_k; \theta_{\text{old}}) + \frac{\epsilon_{t_k}}{\beta} \nabla_x r_p(X_k, t_k) \right) \\ &= \sqrt{2\epsilon_{t_k}\Delta t} Z_k + \Delta t \left(\frac{\epsilon_{t_k}}{\beta} \nabla_x r_p(X_k, t_k) \right). \end{aligned} \quad (62)$$

This derivation mathematically confirms that the guided sample X_{k+1} deviates from the unguided teacher's expectation exactly by the reward gradient term.

Student Process (Optimization Objective). The student policy is defined **without** explicit reward guidance:

$$\mu_\theta(X_k, t_k) = X_k + \Delta t \cdot \mathcal{D}_{\text{flow}}(X_k, t_k; \theta). \quad (63)$$

$$\log \pi_\theta(X_{k+1}|X_k) = C_k - \frac{1}{4\epsilon_{t_k}\Delta t} \|X_{k+1} - \mu_\theta(X_k, t_k)\|^2. \quad (64)$$

We substitute the same sample X_{k+1} from Equation (60) into this residual term:

$$\begin{aligned} X_{k+1} - \mu_\theta(X_k, t_k) &= \left(X_k + \Delta t \left[\mathcal{D}_{\text{flow}}^{\text{old}} + \frac{\epsilon_{t_k}}{\beta} \nabla_x r_p \right] + \sqrt{2\epsilon_{t_k}\Delta t} Z_k \right) - \left(X_k + \Delta t \mathcal{D}_{\text{flow}}^\theta \right) \\ &= \sqrt{2\epsilon_{t_k}\Delta t} Z_k + \Delta t \left(\mathcal{D}_{\text{flow}}(X_k, t_k; \theta_{\text{old}}) - \mathcal{D}_{\text{flow}}(X_k, t_k; \theta) + \frac{\epsilon_{t_k}}{\beta} \nabla_x r_p(X_k, t_k) \right) \\ &= \sqrt{2\epsilon_{t_k}\Delta t} Z_k + \Delta t \left(\left[\left(1 + \frac{t_k \epsilon_{t_k}}{1 - t_k} \right) u_{\theta_{\text{old}}} - \frac{\epsilon_{t_k}}{1 - t_k} X_k \right] - \left[\left(1 + \frac{t_k \epsilon_{t_k}}{1 - t_k} \right) u_\theta - \frac{\epsilon_{t_k}}{1 - t_k} X_k \right] + \frac{\epsilon_{t_k}}{\beta} \nabla_x r_p \right) \\ &= \sqrt{2\epsilon_{t_k}\Delta t} Z_k + \Delta t \left[\left(1 + \frac{t_k \epsilon_{t_k}}{1 - t_k} \right) (u_{\theta_{\text{old}}}(X_k, t_k) - u_\theta(X_k, t_k)) + \frac{\epsilon_{t_k}}{\beta} \nabla_x r_p(X_k, t_k) \right]. \end{aligned} \quad (65)$$

The equation shows that the student velocity u_θ is forced to match the behavior velocity $u_{\theta_{\text{old}}}$ *plus* the direction induced by the process reward gradient $\nabla_x r_p$. This effectively distills the reward information directly into the weights of the flow network.

Remark on Inference/Deployment. In this distillation framework, the optimization objective explicitly forces the student flow network u_θ to internalize the guidance signal provided by the teacher. Consequently, the student model functions independently in deployment. It generates high-reward trajectories relying solely on its learned velocity field, thereby *completely eliminating* the need to compute $\nabla_x r_p$ or load the reward model. This results in a streamlined inference process that is operationally identical to the base model but with aligned behavior.

E.3. Empirical Comparison of Inference Protocols

We evaluate three distinct inference protocols derived from our framework to understand the trade-offs between alignment quality, computational cost, and deployment complexity. All variants utilize the same HunyuanVideo-14B backbone.

1. **Inference RGG:** Using the Standard Optimization model and *retaining* the RGG ($\nabla_x r_p$) during inference. This requires loading the LRM.
2. **Implicit:** Using the Standard Optimization model but *discarding* the RGG during inference.
3. **Distilled:** Using the model trained via the Policy Distillation objective, sampled without RGG.

Table 6. Comparison of Inference Protocols. We compare three variants derived from our framework. Ours (Distilled) achieves the best alignment performance by explicitly supervising the flow network to mimic the guided trajectory. Crucially, it eliminates the need for an external LRM during inference, offering the best trade-off between quality and efficiency. Note that the Inference RGG variant encounters out-of-memory (OOM) errors on a single H20 GPU at high resolutions and frame counts ($81 \times 640 \times 640$), rendering it impractical for standard deployment scenarios.

| Method Variant | Training Objective | Inference Guidance | External LRM | VBench2 Total |
|-------------------------|--------------------------|----------------------------|-----------------|---------------|
| Ours (Implicit) | Standard (Equation (57)) | w/o RGG | None | 53.71 |
| Ours (Inference RGG) | Standard (Equation (57)) | w/ RGG ($\lambda = 0.1$) | Required | OOM |
| Ours (Distilled) | Distill (Equation (64)) | w/o RGG | None | 54.24 |

Analysis. As presented in Table 6, the **Policy Distillation** variant demonstrates better performance than the standard implicit baseline. Notably, the “Inference RGG” mode, which retains the RGG during inference, encounters out-of-memory (OOM)

errors when deployed on a single NVIDIA H20 GPU (96 GB VRAM) without model parallelism. This limitation arises from the substantial memory overhead introduced by concurrently loading both the video generation backbone and the external LRM, compounded by the need to compute and backpropagate reward gradients through high-resolution, high-frame-count video latents. This practical constraint underscores the critical importance of the distillation approach: the distilled model explicitly internalizes the preference signal into its velocity field via the student-teacher objective, enabling deployment with the same memory footprint as the base model. This explicit distillation further enables the model to capture the guided dynamics more accurately than the “Implicit” baseline, achieving state-of-the-art alignment scores. Given that it eliminates the dependency on the external LRM, avoids the prohibitive memory requirements of runtime guidance, and delivers the highest generation quality, we adopt the **Distilled** formulation as our primary method for all experiments.

F. Implementation Details.

Our framework is implemented using PyTorch (Paszke et al., 2019). For distributed training, we utilize Fully Sharded Data Parallel (FSDP) (Zhao et al., 2023) with a “Full Sharding” strategy to efficiently manage the memory footprint of the 14B-parameter backbone. The training is conducted on a high-performance cluster consisting of 5 nodes, each equipped with 8 NVIDIA H800 GPUs (80GB VRAM) and an Intel(R) Xeon(R) Platinum 8476C CPU. We employ gradient checkpointing and mixed-precision training (bf16) to further optimize resource usage. With a per-device batch size of 1 and gradient accumulation steps of 4 across 40 GPUs, the effective global batch size is 160.

Table 7. Hyperparameters and Implementation Details. We list the detailed configuration used for training Euphonium with the HunyuanVideo-14B backbone. Note that the sampling configuration differs between the training rollout phase and the final evaluation.

| Category | Hyperparameter | Symbol | Value |
|-----------------------------|-------------------------------|----------------------|-----------------------------------|
| Model Architecture | Backbone Model | u_θ | HunyuanVideo (Kong et al., 2024) |
| | Process Reward Model (PRM) | r_p | Latent DiT (8 Layers) |
| | Outcome Reward Model (ORM) | r_o | InternVL3-1B (Zhu et al., 2025) |
| | VAE Compression Factor | - | $8 \times 8 \times 4$ |
| Training Configuration | Optimizer | - | AdamW (Loshchilov & Hutter, 2017) |
| | Precision | - | bf16 |
| | Learning Rate | η | 1×10^{-6} |
| | Weight Decay | - | 1×10^{-4} |
| | Batch Size (per Device) | - | 1 |
| | Gradient Accumulation Steps | - | 4 |
| | Total GPUs | - | 40 |
| | Total Training Steps | - | 250 |
| Sampling (Training Rollout) | Sampling Steps | T | 16 |
| | Group Size (per prompt) | G | 8 |
| | Resolution | $H \times W$ | 480×480 |
| | Number of Frames | F | 32 |
| | Time Shift | s | 5.0 |
| Sampling (Evaluation) | Sampling Steps | T | 30 |
| | Resolution | $H \times W$ | 640×640 |
| | Number of Frames | F | 81 |
| Reward-Gradient Guidance | Guidance Scale | λ | 0.1 |
| | KL Regularization Coefficient | β | 3.125 |
| | Exploration Noise | ϵ_t | 0.3125 |
| | Guidance Window (Steps) | - | $8 \rightarrow 16$ (Latter Half) |
| | Guidance Window (Time) | t | $[0.5, 1.0]$ |
| GRPO Optimization | Process Reward Weight | - | 1.0 |
| | Outcome Reward Weight | - | 1.0 |
| | Clip Parameter | ε_{clip} | 1×10^{-4} |